INTERNATIONAL JOURNAL FOR NUMERICAL METHODS IN FLUIDS
Int. J. Numer. Meth. Fluids 2001; **36**: 687–709 (DOI: 10.1002/fld.152)

High-order Cartesian grid method for calculation of incompressible turbulent flows

J. Gullbrand, X. S. Bai* and L. Fuchs

Department of Heat and Power Engineering, Division of Fluid Mechanics, Lund Institute of Technology, Lund, Sweden

SUMMARY

A high-order wall treatment is proposed and implemented into a Cartesian grid method and the wall treatment is evaluated for incompressible turbulent flows. The Cartesian grid method employs a sequence of locally refined, uniformly spaced, Cartesian grids. In order to achieve a high-order accuracy, a wall treatment procedure has been developed for arbitrarily shaped geometries. The procedure consists of high-order Lagrangian polynomial interpolations and extrapolations for determining the dependent variables around the wall boundaries. The wall treatment procedure and the Cartesian grid method are used together with a highly efficient multi-grid acceleration method and a local grid refinement strategy for optimal distribution of the grid points. The high-order Cartesian grid method is evaluated using test functions as well as for laminar and turbulent flows. The proposed approach maintains the high-order discretization and yields high-order accuracy of the numerical results. Large eddy simulation of a turbulent swirling flow indicates that the high-order wall treatment leads to significantly different results from those calculated using a low-order piecewise constant wall description. The differences in the results are smaller at a low level of turbulence near the inlet region, but become significant in the region far away from the inlet where the turbulence is more intense. In the latter situation the effect of the wall treatment is as important as the choice of the subgrid scale stress model. Copyright © 2001 John Wiley & Sons, Ltd.

KEY WORDS: Cartesian grid method; high-order wall treatment; large eddy simulation; turbulence

1. INTRODUCTION

Large eddy simulation (LES) of turbulence has several advantages and disadvantages as compared to models within the Reynolds averaged Navier–Stokes (RANS) framework. The main advantages of LES are related to its potential to have a universal behavior if the spatial resolution is adequate. It becomes arbitrarily accurate as the grid is refined, and is highly appropriate for flows which include laminar and transitional regions and/or which include a

* Correspondence to: Department of Heat and Power Engineering, Division of Fluid Mechanics, Lund Institute of Technology, S-221 00 Lund, Sweden.

Received July 1999
Revised February 2000

strong interaction between turbulence and coherent structures of the flow. LES requires by nature high spatial resolution and temporal resolution which implies that the computational times are often long. RANS based models, on the other hand, require much less spatial resolution since the averaged variables are much more smoother than the instantaneous ones. If the flow is statistically stationary, no time-evolution has to be followed.

In general, the main sources of errors in LES are the spatial resolution and the effects of the subgrid scale (SGS) models. For spectral methods, aliasing errors may also contribute to the total error. The spatial resolution is essential for all discrete approximations. It is meaningless to use asymptotically superior discretization schemes if the scales of the dependent variable are unresolved. For polynomial based approximations, such as finite differences, finite volumes and finite elements, higher order approximations are of any significance only if the spatial resolution inside the domain *and* on the boundaries is adequate. One of the aims of this paper is to assess the relative importance of the errors in applying wall boundary treatment as compared to the SGS modeling effects.

Most of the efforts in LES research have been to develop general SGS models. One of the first models was proposed by Smagorinsky [1] and more recent models are the stress similarity model [2,3] and dynamic models [4,5]. The evaluation and comparison of different models have been performed for homogeneous isotropic turbulence, e.g. by Clark *et al.* [6] and Fureby *et al.* [7].

There is a general belief that finite difference errors can be minimized by using higher-order schemes [8]. This is of course correct when the ratio of the grid size to the local length scales is much smaller than unity. This is not the case in LES. However, when the spatial resolution improves, the energy content of the small scale eddies is small and the error made by the inadequate resolution is relatively small. This argument would imply that the error in the energy reduces in the time average sense as $O(h^{2/3})$. Thus, the main effect of the high-order discretization is on scales that are significantly larger than the grid size. The situation is similar also for spectral methods. Therefore, for engineering problems, local polynomial based discretization methods, such as the finite difference, finite element and finite volume methods, are mostly used. Low-order schemes such as second-order finite difference schemes were shown to cause a high level of discretization error [8], at least for not very fine grids. High-order schemes are preferable for LES in order to accurately simulate the details of the large scale effects.

High-order schemes are easier to implement in rectangular Cartesian grids than on general body-fitted grids. Other advantages associated with Cartesian grids are that the grid generation is fast, the computational storage requirements are small and there is considerably less computational effort per computational cell when compared to the same equations expressed on a body-fitted grid. In addition, the convergence properties of the algorithm are often better in Cartesian grids. These are all desired features in LES, in order to decrease the long computational times. One of the main difficulties when using Cartesian grids is handling arbitrary shaped boundaries, i.e. the representation of the boundaries and the implementation of the boundary conditions. To overcome this difficulty different methods have been proposed [9–12]. The different approaches for handling the boundary conditions are called *Cartesian grid methods*.

In this paper, a high-order Cartesian grid method is proposed for arbitrarily shaped geometries and it is evaluated together with different SGS stress models. Arbitrarily shaped boundaries may be represented by piecewise 'steps', which may differ from the exact boundary by, at most, the size of a cell. The step wall is first-order accurate in describing the geometry. Therefore, when very fine cells are used the boundaries are well approximated [13]. Alternatively, the shape and size of the cells near the boundaries can be adjusted so that the grid points are located on the boundaries. This leads to non-uniform arbitrary shaped cells near the walls and a second-order description of the shape of the boundary. The smallest cells limit the allowed time steps and thus the numerical efficiency of most numerical scheme [14]. This difficulty may be remedied, for example by using an adaptive local grid refinement near the boundaries [10,15,16]; or combining the small cells with neighboring ones by a merging procedure, as suggested by Quirk [9], Coirir and Powell [17]. Most of the methods have been applied to two-dimensional inviscid flow calculations. The extension of these methods to three-dimensional geometries is tedious and associated with difficulties. Forrer and Jeltsch [11] illustrated a different approach. A higher-order wall treatment based on uniform grids at the walls is described and a wall reflection procedure is proposed. However, the method has only been implemented for two-dimensional inviscid flows with symmetry wall boundary conditions.

It should be pointed out that even when the wall boundary is aligned with a grid line the accuracy of the wall treatment is problematic. The resolution near a solid wall is very important in turbulent flows, since the shear of boundary layers is a major source of generation of turbulence at short distances from the wall, $5 < y^+ < 100$. The burst generated inside the boundary layer is ejected away from the wall and 'external' fluid is swept into the boundary layer. To resolve such phenomena, the spatial resolution of the grid has to be adequate. The resolution can be increased by introducing local grid refinements [18]. Since the length scales are different in the normal and parallel directions to the wall, anisotropic local grid refinements can be used instead. Such techniques have been utilized by Li and Fuchs [19] and by Pierce and Moin [20]. Once the spatial resolution closest to the boundary is fine enough and the instantaneous profile is linear, the present high-order Cartesian grid method introduces no truncation errors due to boundary conditions.

Our proposed high-order Cartesian grid method is easy to implement and numerically efficient. Similar to the approach of Forrer and Jeltsch [11] a uniform rectangular Cartesian grid is used throughout the flow field. The computational domain is extended to reach outside the curved wall boundaries. The governing equations are not solved in the cells that are intersected by the wall or are outside the domain. Instead, the dependent variables are interpolated or extrapolated to these cells. The interpolation and extrapolation schemes satisfy also the boundary conditions at the correct location.

The high-order Cartesian method and the low-order step-wall representation are evaluated for test functions as well as for laminar and turbulent isothermal incompressible flows. The accuracy of the solution is determined in a laminar Poiseuille flow. In a turbulent incompressible swirling flow, the influence of the SGS models are compared to the influence of the different wall boundary treatment methods. This demonstrates the relative importance of the high-order Cartesian grid method on the LES results.

2. GOVERNING EQUATIONS

The governing equations for an isothermal incompressible viscous flow are the continuity equation and Navier–Stokes equations. In a Cartesian co-ordinate system, the equations can be written as

$$\frac{\partial u_j}{\partial x_j} = 0 \tag{1}$$

$$\frac{\partial \rho u_i}{\partial t} + \frac{\partial \rho u_i u_j}{\partial x_j} = -\frac{\partial p}{\partial x_i} + \mu \frac{\partial^2 u_i}{\partial x_j^2} \tag{2}$$

where ρ is the density, t is time, p is the pressure and μ is the laminar viscosity. u_i $(i = 1, 2, 3)$ are the velocity components along the x_i co-ordinates. In the above equations, Einstein's summation convention is used.

The equations can be solved numerically for laminar flows. For turbulent flows the numerical solution is called direct numerical simulation (DNS) if all the length scales and time scales are resolved. For high Reynolds number flows, DNS is not feasible due to the lack of computational resources. A more suitable approach for high Reynolds number flows is the LES approach. In LES, all the larger eddies are resolved and only the smaller ones are modeled.

The system of Equations (1) and (2) requires d boundary conditions, where d is the dimension of the problem.

2.1. LES equations

In LES, the space filtering approach is applied to the governing equations. A filter function G with the filter width Δ_f is applied to a flow variable ϕ to obtain a filtered flow variable $\bar{\phi}$, according to

$$\bar{\phi}(x, t;\ \Delta_f) = \int_{-\infty}^{\infty} G(x - x';\ \Delta_f)\phi(x', t)\, \mathrm{d}x' \tag{3}$$

The space filtering approach divides the flow field into two different groups of length scales. The first group consists of eddies that are larger than the applied filter width and therefore are fully resolved. The second group contains the small unresolved eddies.

The space filtered continuity equation (1) and Navier–Stokes equation (2) for an isothermal incompressible fluid can be written as

$$\frac{\partial \bar{u}_j}{\partial x_j} = 0 \tag{4}$$

$$\frac{\partial \rho \bar{u}_i}{\partial t} + \frac{\partial \rho \bar{u}_i \bar{u}_j}{\partial x_j} = -\frac{\partial \bar{p}}{\partial x_i} + \mu \frac{\partial^2 \bar{u}_i}{\partial x_j^2} - \frac{\partial \tau_{ij}}{\partial x_j} \tag{5}$$

where τ_{ij}, the SGS stress tensor, represents the interaction between the unresolved eddies and the resolved ones.

The definition of the SGS stress tensor is

$$\tau_{ij} = \rho(\overline{u_i u_j} - \bar{u}_i \bar{u}_j) \tag{6}$$

The stress tensor cannot be expressed by the resolved variables because it consists of the unknown term $\overline{u_i u_j}$. Therefore, the SGS stress tensor has to be calculated by an appropriate model.

The number of boundary conditions for the filtered equation system with Equations (4) and (5) is the same as the dimension of the problem. It should be noted that by filtering the governing equations also the boundary conditions should be filtered. Filtered boundary conditions have not been used in this work. By applying the unfiltered conditions of no-slip conditions at the wall, the boundary conditions are accurate to second-order of the filter width.

2.2. SGS stress models

The role of a SGS model is to account for the SGS stress using the resolved flow variables. Different SGS models have been proposed. The Smagorinsky model [1] was shown to be absolute dissipative, which implies that turbulent kinetic energy is transferred from large scales to small ones. It accounts only for the viscous dissipation of the unresolved scales. However, the instantaneous energy transfer in the opposite direction, i.e. from small to large length scales (back-scatter), is substantial in turbulent flows. More recent models, such as the stress similarity models (SSM) [2,3] and the dynamic models [4,5], have been shown to allow for back-scatter.

In our simulations two SGS models have been used: an implicit model (IMM) and a SSM.

2.2.1. Implicit model. An IMM uses no explicit SGS model. The finite difference error of the discretization scheme acts as a SGS model. This type of approach asymptotically becomes DNS when the numerical grid resolves the finest turbulent length scale, i.e. the Kolmogorov scale. The basic arguments behind IMM are based on the understanding of the roles of the SGS models. Two main roles of the SGS models can be identified: (1) to account for the dissipation of energy at the end of the turbulent energy cascade and (2) to account for the effects of the unresolved scales. The dissipation effects are mandatory. Energy is transferred from the large length scales to the small scales and it should not be accumulated there. The molecular viscosity is inadequate for draining energy at the rate by which it is being extracted from the large scales. Since all numerical methods have to be dissipative using either the molecular dissipation or some numerical dissipation to not accumulate perturbations. The dissipative role of the SGS terms can be replaced by a numerical one provided that it does not dissipate energy from the larger scales. If the IMM approach is used, the second role of the SGS terms cannot be accounted for in a physical manner. Yet, when the spatial resolution is fine enough, the SGS model induced back-scatter as well as the numerical dissipations do not affect the larger scales of motion. In the literature, the concept of 'monotone integrated LES' (MILES) has been used for a scheme in which no explicit SGS model is used [21]. Our

numerical scheme is not monotone, yet it can function well both for its dissipative role and in some sense in its dispersive (non-physically related 'back-scatter') role. The accuracy and applicability of this approach for modeling the SGS effects may require, however, additional investigation for different cases. In this paper, IMM results are compared with SSM results so that the relative importance of the effects of the SGS models and the wall treatment can be assessed.

2.2.2. SSM. A stress similarity model is based on the assumption of similar behavior between the resolved small scale stresses and the unresolved ones. A resolved stress is calculated by applying an additional filter function to the resolved variables ($\hat{\bar{\phi}}$). The unresolved SGS stress is estimated by the resolved one. The stress similarity model as proposed by Liu *et al.* [3] is used in this work. For incompressible isothermal flows the model has the following form

$$\tau_{ij} - \frac{1}{3}\delta_{ij}\tau_{kk} = \rho(\hat{\bar{u}}_i\hat{\bar{u}}_j - \hat{\bar{u}}_j\hat{\bar{u}}_i) \tag{7}$$

The model yields back-scatter since it is not absolutely dissipative. Numerically this may lead to instability of the numerical algorithm. This instability reflects the fact that the turbulent kinetic energy, which is transferred in the energy cascade from the large length scales to the small ones, is not dissipated on the small scales. A remedy can be found by using a mixed model, which is a linear combination of the stress similarity model and a purely dissipative term, such as the Smagorinsky model. The Smagorinsky model is of order Δ_f^2, and could be too dissipative. In this work, Liu *et al.*'s SSM is numerically stabilized by the dissipation of the numerical scheme which is of formal order of Δ_f^3.

The additional filter applied in SSM and the filter function and filter width has to be defined. The filter width of the second filter must be wider than Δ_f. In the simulations, the filter is twice as wide as the grid filter, i.e. $\hat{\Delta}_f/\Delta_f = 2$. Applying the second filter to the resolved quantity $\hat{\bar{\phi}}$ can be written as

$$\hat{\bar{\phi}}(x, t;\ \hat{\Delta}_f) = \int_{-\infty}^{\infty} G(x - x';\ \hat{\Delta}_f)\bar{\phi}(x', t)\,\mathrm{d}x' \tag{8}$$

It has been argued that the form of the filter may have a significant influence of LES results [3]. A discussion of different filters can be found in Reference [22]. In this work a discrete approximation of a Gaussian type filter is used, namely

$$\hat{\bar{\phi}}_{ijl} = A \begin{pmatrix} \bar{\phi}_{i-1,j,l} \\ \bar{\phi}_{i,j,l} \\ \bar{\phi}_{i+1,j,l} \end{pmatrix}, \quad A = \frac{1}{6}(1 \quad 4 \quad 1) \tag{9}$$

where $\bar{\phi}_{i,j,l}$ denotes resolved quantity at grid point (i, j, l). The procedure is repeated in all three directions, to yield the final value of $\hat{\bar{\phi}}$.

3. NUMERICAL METHODS

The governing equations are discretized on a Cartesian grid system where the grid points are uniformly distributed in each co-ordinate direction. By this arrangement the numerical efficiency is high and high-order spatial discretizations are easily implemented. Local grid refinements (either isotropic [18] or anisotropic [19]) can be introduced 'statically' or 'dynamically', i.e. adaptively. For complex geometries, a high-order wall treatment is necessary to maintain the high-order discretization close to the walls. The discretization scheme, the high-order wall treatment and the solution procedure are described below.

3.1. The grid system

Cartesian grids can describe a curved surface boundary only approximately. Generally, the walls intersect some cells in the grid, as illustrated by Figure 1. Three types of cells are defined as 'active' cells, 'wall' cells and 'cut' cells respectively. The active cells are those fully within the flow field which do not intersect the wall boundaries, the wall cells are those completely outside the flow field and the cut cells are those which intersect the wall boundaries.

The dependent variables are defined on a staggered grid system. That is, the pressure is defined at the cell center and the components of the velocity vector are defined at the center of the cell surface normal to the velocity component under consideration. The position of the scalars is shown in Figure 1 as point *T*.

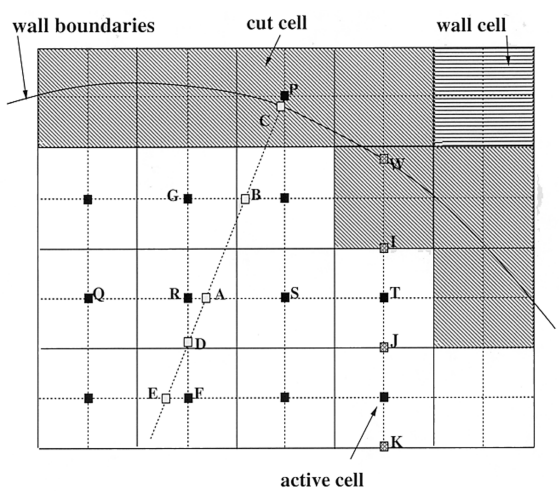

Figure 1. A sketch of the interpolation procedure in a two-dimensional geometry.

3.2. The discretization scheme

The spatial derivatives are discretized by the fourth-order central difference scheme. Denote the second-order and fourth-order central difference approximation to the first-order derivative in the j-direction by δ_j and D_j respectively. By using this notation the discretized continuity equation can be written as

$$D_j\bar{u}_j = 0 \tag{10}$$

The discretized momentum equation uses both a fourth-order (D_j) and a second-order (δ_j) central difference approximation. The discretized momentum equation in the x_i direction can be written as

$$\rho\frac{\partial\bar{u}_i}{\partial t} + L_i(u,p) + \delta_j\tau_{ij} + \delta_j\psi_{ij} = R_i(u,p) \tag{11}$$

where

$$L_i(u,p) = \delta_j\rho\bar{u}_j\bar{u}_i + \delta_i\bar{p} - \mu\delta_j\delta_j\bar{u}_i \quad R_i(u,p) = L_i(u,p) - H_i(u,p) \tag{12}$$

and

$$H_i(u,p) = D_j\rho\bar{u}_j\bar{u}_i + D_i\bar{p} - \mu D_jD_j\bar{u}_i$$

The term $R_i(u,p)$ represents the defect between the low-order and the high-order schemes.

The molecular viscosity leads to adequate dissipation on the smallest scales of turbulence (i.e. about the Kolmogorov micro-scales, η). Since the grid (h) is much larger than the Kolmogorov scale, the dissipation due to molecular viscosity at the grid scale (h) is too small. If the spatial resolution of LES is such that it resolves the Taylor micro-scales (λ), which is mandatory for the IMM approach, then the molecular dissipation is only a small fraction (of the order $O(Re^{-1/2})$) of the total dissipation required for the energy transfer from the resolved scales to the unresolved scales. As discussed above, one of the roles of SGS is to account for that missing dissipation. In the case of IMM this is implicit by the discretization scheme.

For higher Reynolds numbers, when the local cell Reynolds number (Peclet number) is larger than 2, the numerical viscosity is too small and the local scale of the flow cannot be supported by the grid. Therefore, by adding numerical viscosity, the numerical solutions is smoothed to get the scale of the grid. Since it is desired not to reduce the accuracy of the larger scales, higher-order numerical viscosity is preferred. The third-order upwind scheme of Kawamura and Kuwahara [23] offers such a possibility. For a smooth function ($\bar{u}_i$) the leading term of the truncation error is identified as the artificial viscosity term and it is proportional to h^3. This term has the form of

$$\delta_j\psi_{ij} = \frac{1}{4}\rho|\bar{u}_j|h^3\delta_j^4\bar{u}_i \tag{13}$$

where summation in j is performed.

This term may be introduced explicitly if only fourth- (or higher-) order central differences are used for discretizing $H(u, p)$.

The time derivatives are approximated by a three-level, second-order implicit scheme, i.e. for $\bar{u}_i$

$$\frac{\partial \bar{u}_i}{\partial t} \approx \frac{3\bar{u}_i^{n+1} - 4\bar{u}_i^n + \bar{u}_i^{n-1}}{2\Delta t} \tag{14}$$

where Δt is the time step. Superscript n denotes the time after n time steps. Initial condition is given at $n = 0$.

3.3. Wall boundary corrections

In the low-order wall boundary treatment, step wall, cells which centers are outside the flow field, are simply blocked out. These blocked cells include all wall cells and some of the cut cells. The discretized governing equations are not solved in these cells and the wall boundary conditions are applied on the interfaces between the blocked cells and cells inside the flow field. Therefore, a solid wall is represented by piecewise steps. This treatment may introduce an error to the wall location by at most one cell size. The cell size is denoted by h and when $h \to 0$, the piecewise rectangular description of the wall tends to the shape of the wall. It can be shown that at point I in Figure 1, the error in $\bar{u}_i$ is of the order h.

A high-order wall treatment consists of interpolations and extrapolations of the dependent variables to cut cells and some wall cells. The interpolation and extrapolation procedure is constructed in such a way that the boundary conditions at the correct boundary locations are satisfied (Figure 1). In the following, Neumann boundary conditions are used for the pressure and no-slip conditions for the velocity at solid walls.

A scalar is defined at the point P, which is the cell center of a cut cell (Figure 1). Assume that the boundary condition at the wall point (C) is a vanishing normal derivative. The points used for the (one-dimensional Lagrange-) interpolation procedure are P, A, B, D, E, etc. They are all located on a line normal to the wall. In order to determine the values at the points A, B, D, E, etc., the dependent variables at surrounding active cells are used. For example, point A will employ points Q, R, S, T, etc., and point D employs points G, R, F, etc. By setting the boundary condition of the normal derivatives at C to zero, the values of the dependent variables at point P are determined.

The high-order Lagrange interpolation formula is used for each component of the velocity vector. The active cells J, K, etc., are used together with the wall point W, in order to calculate the velocity component at point I. For higher orders of accuracy more points have to be used.

A central issue of the procedure described above is the smoothness of the interpolated variable. 'Noisy' or fluctuating data will result in large errors when high-order interpolation schemes are used. In LES, the flow field is fluctuating by nature and there is a clear risk for loss of accuracy. However, if the grid is fine enough, improved accuracy can be obtained unless too high an interpolation order is used. Ideally, at least two grid cells in the viscous sublayer is desired, in order to be able to apply a low interpolation order. This would also eliminate the difficulties associated with the fluctuating data.

3.4. Solution method

The basic solver uses the discretization discussed in Section 3.2. For stationary problems, the momentum equations and the continuity equations are relaxed iteratively in the framework of a multi-grid method. During the relaxation of the continuity equation, the pressure and the velocities are updated through a distributive Gauss–Seidel (DGS) scheme [24–26]. For the time-dependent case, the discrete problem is updated using the implicit scheme described in the section 'The discretization scheme'. In each time step, the same multi-grid procedure is used as in the stationary solver. In all the relaxation steps, the lowest-order discrete scheme is used. Higher order accuracy is attained by using a single/few-steps defect correction method. To enhance the numerical efficiency, a defect correction scheme as given by Equation (11) is applied. It is more efficient to correct the low-order solution to a higher order than solve the high-order discretized equations directly. The low-order scheme has usually better stability properties, compared to the high-order one, by introducing only the defect of the higher-order scheme.

For stationary problems, R, the defect (difference) between the residuals of the higher and the lower order operators, in Equation (11), can be computed explicitly in each iterative step and the problem is resolved using the lower order operator. In the Appendix, it is shown that if the discretization order of L_i and H_i are two and four respectively, a single step of defect calculation is enough to reach the fourth-order accuracy. If the order of L_{i} is one, then three defect-correction steps are required.

In the case of time dependent flows, the 'single step' defect correction scheme, once in each time-step, yields a higher-order accuracy, with the stability properties of the lower-order operator. If the accuracy of the single step defect correction is adequate, the procedure will be to compute the defect at the beginning of each time step. This defect is not updated during the implicit step. The accuracy of the approach will be of the formal order of $O(\Delta t h^2)$ for the continuity and the momentum equations, if central differences are used. This accuracy is adequate for most LES applications. Since, fluctuations of eddies of the same size as a computational cell is desired, the time step is of the same order as the computational cell and most often smaller, if the local velocity is assumed to be of order unity. Thus, this single defect step approach is as accurate as the artificial viscosity term of the spatial discretization, Equation (13), or the SGS term, Equation (6). Higher-order accuracy may be attained by updating the defect in a fractional step approach, i.e. in a manner corresponding to the few-steps defect correction of Appendix A.

4. RESULTS AND DISCUSSION

In order to analyze the proposed high-order wall treatment in the Cartesian grid method, three different cases are examined. First, the order of discretization is examined by employing a test function. The second test case is a laminar, steady, infinitely long pipe flow. The laminar flow field has an exact solution whereby the numerical error can be directly computed. In this study, the behavior of different wall treatments on the solution accuracy

is studied. In the third test case, the high-order Cartesian wall treatment is applied to LES of the inlet region of a swirling turbulent flow in a cylindrical combustion chamber. The time-averaged flow field computed by using different wall treatment methods and SGS models are compared, in order to assess the relative accuracy of the wall treatment and its importance relative to the effects of the chosen SGS model.

4.1. Influence of wall treatment on the order of discretization

In order to investigate the influence of wall treatment on the order of discretization, test functions are used. The functions are applied to cylindrical shaped pipe with a radius R (test case 1).

The test functions for the velocity and pressure field are as follows

$$u(x,r) = v(x,r) = w(x,r) = \sin\left\{\frac{\pi}{2}\left[1-\left(\frac{r}{R}\right)^2\right]\right\}\cos[x(1-x)]$$

$$p(x,r) = \sin\left[\frac{\pi}{2}\left(\frac{r}{R}\right)^2\right]\cos[x(1-x)] \tag{15}$$

where r is the radial co-ordinate and x is the axial co-ordinate. The test functions for the velocity components satisfy the no-slip condition at the wall boundary ($r = R$) and the pressure term fulfills the Neumann condition $\partial p/\partial r = 0$ at the wall boundary. At the boundary cells, the velocity components are either obtained by the proposed higher-order wall treatment or by the step-wall treatment.

The L_2-norms of the truncation errors are studied and they are defined according to

$$\|R_\phi^h\| = \left\{\frac{1}{N_C}\sum_{i=1}^{N_C}[L(\phi) - L^h(\phi)]^2\right\}^{1/2} \tag{16}$$

where $L(\phi) = 0$ represents the differential Navier–Stokes equations and $L^h(\phi) = 0$ represents the discretized governing equations. N_C is the total number of active cells that have been used to calculate the L_2-norm and h is the cell size. The L_2-norm, $\|R_\phi^h\|$, is a function of h and it can be used to estimate the discretization order.

The L_2-norm of the truncation error for the continuity equation is shown in Figure 2. The solid line represents fourth-order discretization, $\|R_\phi^h\| \sim O(h^4)$. The squares represent the results using fourth-order interpolations for velocity components at the cut cells and wall cells. As seen, the fourth-order accuracy is maintained by using the higher-order wall treatment. The step-wall approximation, denoted by the circles in the figure, leads to low-order accuracy, $\|R_\phi^h\| \sim O(h^{0.5})$.

The L_2-norm of the truncation error for the axial momentum equation is shown in Figure 3. Similarly, it can be seen that the higher-order wall treatment maintains the order of discretization, $O(h^3)$, while step-wall approximation yields a low-order of accuracy, $O(h^{0.5})$.

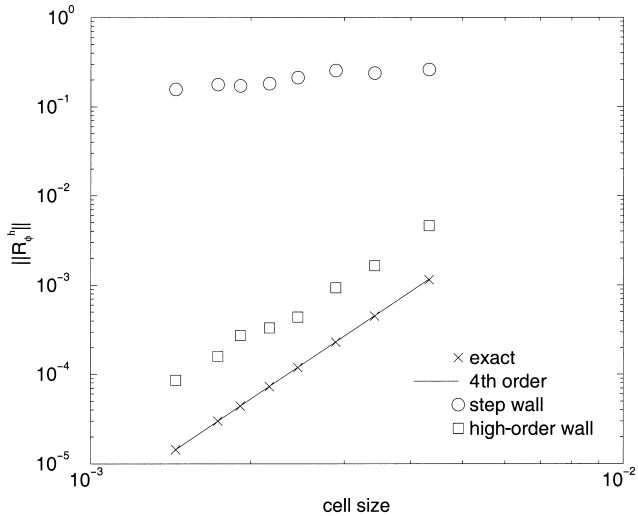

Figure 2. Dependence of $\|R_\phi^h\|$ of continuity equation on the cell size h (test case 1).

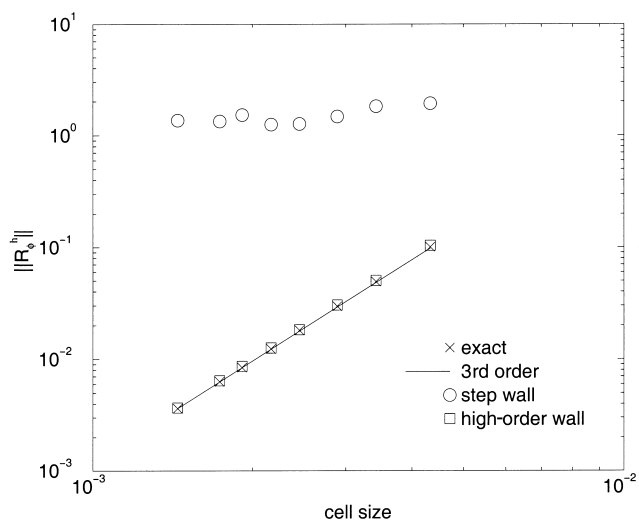

Figure 3. Dependence of $\|R_\phi^h\|$ of the axial momentum equation on the cell size h (test case 1).

4.2. Error propagation in laminar pipe flows

A fully developed laminar pipe flow is considered (test case 2). As seen from the above results, different treatments of the walls lead to different orders of the discretization in the active cells. The Reynolds number of the flow is 10 and the exact solution of the axial velocity component is a parabolic profile.

The numerical errors in the results calculated using the step-wall treatment are shown in Figure 4. The error, defined as the root-mean-square (rms) of the differences between computed values and exact solutions, is calculated using all the active cells in a cross section and the result is denoted by circles in the figure. The error decreases linearly as a function of cell size h, even though third-order discretization is used in all active cells. The linear behavior is also seen when the error is calculated for the first active cell layer near the walls, diamonds in the figure.

When the higher-order wall treatment is applied to the flow field the numerical error vanishes to machine accuracy, single precision $O(10^{-6})$, since this velocity profile leaves no discretization errors (Figure 5). These results indicate that the lower-order treatment of the boundary conditions results in lower-order accuracy not only near the walls but also globally.

4.3. Boundary treatment in a turbulent flow

The influence of wall treatments on LES results of the near inlet region of a turbulent swirling flow in a pipe is investigated (test case 3). Both time-averaged mean and fluctuating properties are examined. Also, the influence of the SGS model is investigated by applying the IMM and the SSM.

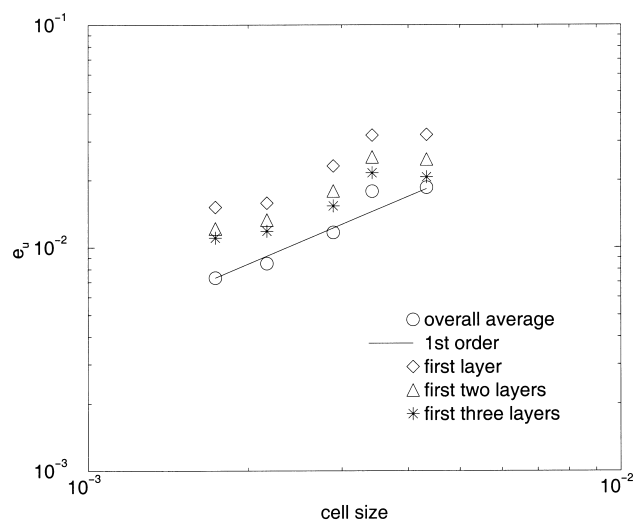

Figure 4. Numerical error as a function of the cell size h. Calculations are performed using the low-order wall treatment (test case 2).

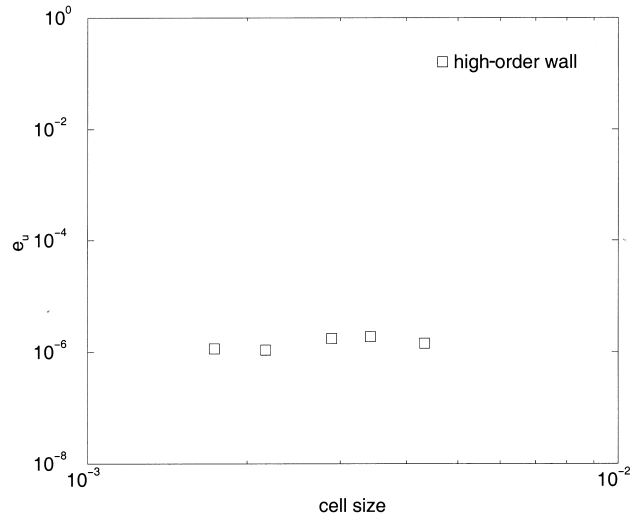

Figure 5. Numerical error as a function of the cell size h. Calculations are performed using high-order wall treatment (test case 2).

4.3.1. Flow field description and initial field. A swirling turbulent co-annular flow in a cylindrical combustion chamber geometry is examined. The cylinder diameter is $D = 12$ cm and there are two inlets. One circular inlet is placed in the center with an inlet flow speed of 1 m s^{-1} and the other is a co-annular inlet with a flow speed of 20 m s^{-1}. The swirl number of the annular inlet is 0.3 and there is no swirl at the circular inlet. The fluid supplied in both inlets is air with inlet temperature 298 K and atmospheric pressure, 1 atm. This combustor was employed in an experimental study by Owen *et al.* [27], in which methane was supplied through the center circular inlet, at a similar speed and a diffusion flame was formed in the chamber.

The boundary condition at the solid wall is the no-slip condition for the velocities. It is implemented by the high-order wall treatment procedure. At the inlet, the magnitudes and profiles for the velocities are given. In order to generate turbulent fluctuations at the inlet, a white noise perturbation of 5 per cent of the inlet speed is introduced. The values of dependent variables at the outflow boundaries are set further downstream to vanishing gradient conditions. The outlet boundary is placed far downstream from the region of interest to not influence the results.

The computational domain is limited to the near inlet region $x < 2D$. In order to obtain more accurate outflow boundary conditions at $x = 2D$, a global coarse grid, double mesh spacing, on a larger range ($x = 4D$) is used. The dependent variables at the outlet boundaries at $x = 2D$ of the fine grid are obtained by interpolations from the solution on the global coarse grid. The global grid is further coarsened twice, thus three global multi-grid levels are used. A sketch of the flow field and the locally refined grid is shown in Figure 6. The grid size of the local finest grid is about 3 mm in the axial direction (x) and 1.5 mm in other directions (y, z). About half a million grid points are used.

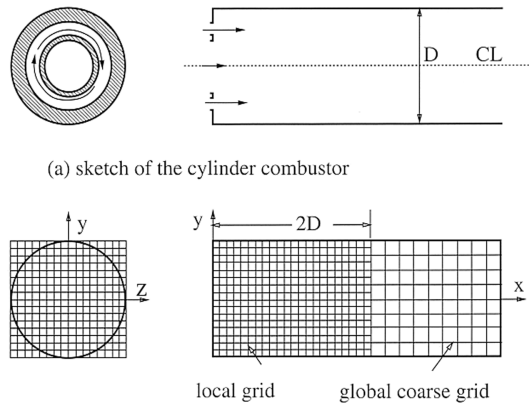

Figure 6. A sketch of the cylinder combustor (test case 3) and the Cartesian grid system.

The initial flow field is obtained by running LES using the simpler step-wall treatment and the SGS model IMM, starting from a zero velocity flow field. When the number of time steps increases, the flow field converges to statistically stationary. The convergence to the statistically stationary flow is examined by the time-averaged mean and variance of the flow variables. After a large number of time steps ($\sim 10^4$), no variations of the time-averaged variables are observed.

4.3.2. Performance of the higher-order wall treatment. The computational times required for the higher-order wall treatment and the lower-order step-wall treatment are roughly the same. The reasons are that a fixed geometry is used in the simulations and all interpolation coefficients are computed only once. The interpolation coefficients depend upon the geometry. For problems with moving walls, the coefficients have to be recalculated in each time step and the higher-order wall treatment is expected to be relatively more expensive.

To be able to resolve the fluctuations of the resolved eddies the cell based CFL number, $\Delta t V/h$, where Δt is the time step and V is the characteristic velocity scale (20 m s^{-1}), is taken to be 0.1.

Both third-order and fourth-order Lagrangian interpolations for the velocity components are found to be numerically stable. The actual order of the PDE discretization near the wall is one order less than the order of the Lagrangian interpolation. Therefore, near the walls second-order accuracy of the discretization is obtained if third-order interpolations are used. Higher-order schemes than second-order near the walls are difficult to motivate primarily due to the fluctuating character of the velocity field in LES. This might also be the situation in some laminar flow situations when the machine round-off or convergence introduces fluctuations. On the other hand, if the viscous sublayer closest to the walls is well resolved, the velocity profile is linear and therefore even linear interpolation is adequate. Liu *et al*. [28] have shown that second-order near-wall treatment is sufficient for simulation of the turbulent transition process.

An instantaneous velocity vector field at $1.5D$ downstream from the inlet is shown in Figure 7. The results are calculated using SSM with and without high-order wall treatment. On the left part of the figure the results related to the higher-order wall treatment is depicted. The no-slip boundary condition at the wall boundary is correctly fulfilled by using the high-order wall interpolations. The right part of the figure shows that the no-slip boundary condition is fulfilled at a piecewise constant step-wall boundary.

4.3.3. The time-averages of the flow field. The time-averaged velocity components in the axial, azimuthal and radial directions and the mean fluctuating value of the axial velocity component at several distances downstream from the inlet plane are shown in Figures 8 and 9. The time-averaged flow field is obtained by applying time average operation on the time dependent LES results, i.e.

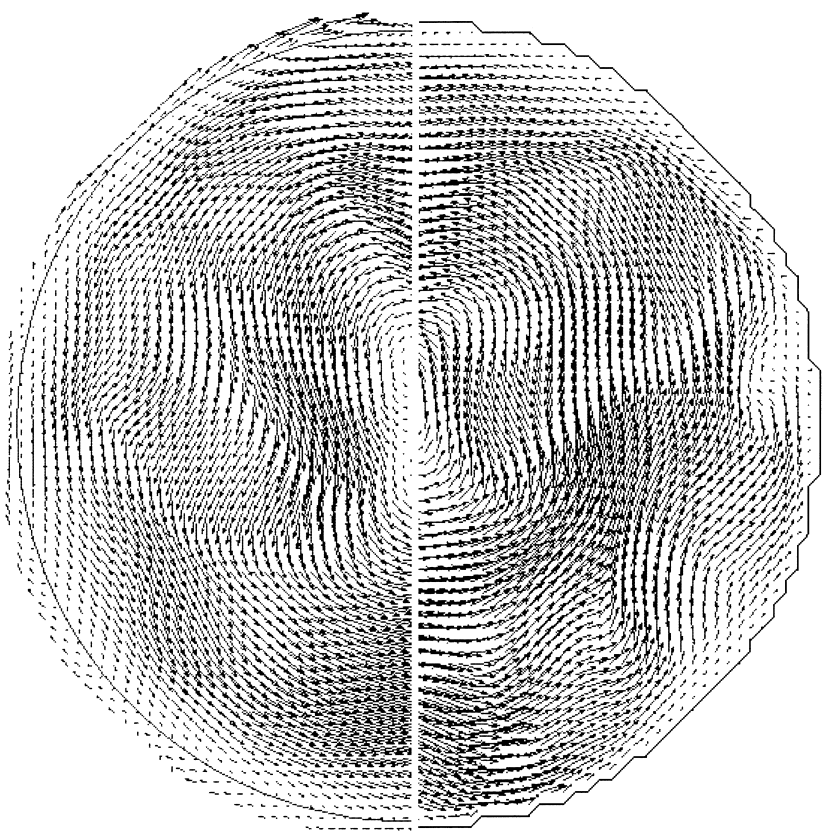

Figure 7. Instantaneous velocity vector field at cross section $x/D = 1.5$. Left figure computed with the high-order wall treatment and SSM and right figure computed with the step wall and SSM (test case 3).

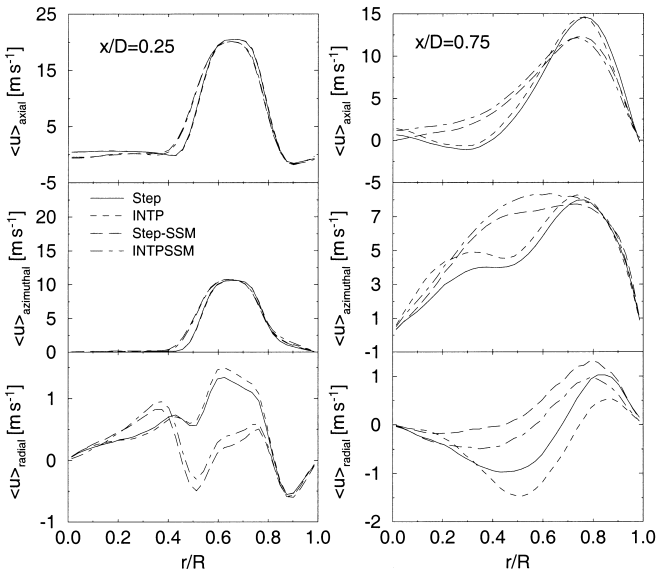

Figure 8. Time-averaged mean velocity components computed using different wall treatment methods and SGS models (test case 3). Step denotes the low-order step-wall treatment with IMM; INTP denotes the high-order wall treatment with IMM; Step-SSM denotes the low-order step-wall treatment with SSM, and INTPSSM denotes high-order wall treatment with SSM.

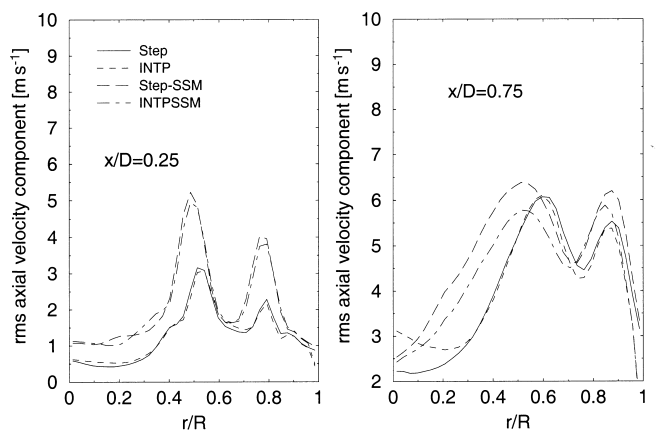

Figure 9. Root-mean-square axial velocity component computed using different wall treatment methods and SGS models (test case 3). Notation as in Figure 8.

$$\langle \bar{\phi} \rangle = \frac{1}{N_t} \sum_{n=1}^{N_t} \bar{\phi}^n, \qquad \bar{\phi}_{rms} = \sqrt{\frac{1}{N_t} \sum_{n=1}^{N_t} (\bar{\phi}^n - \langle \bar{\phi} \rangle)^2}$$

The total number of time steps N_t used in our simulations is about 10^4.

The influence of SGS models and numerical methods, i.e. boundary treatment, is clearly seen in Figures 8 and 9. The time-averaged radial velocity component computed using step-wall treatment differs significantly from the results calculated using high-order wall treatment. The differences in axial and azimuthal components are smaller. The influence of SGS models on the time-averaged flow field is more significant than the influence of the wall treatment, in particular at near-inlet regions, e.g. $x/D = 0.25$ plane, before turbulence is fully developed. Further downstream, the effects of SGS models and wall boundary treatment are of the same order of magnitude and importance. The axial mean fluctuating velocity component, u_{rms}, shows a similar trend. At the cross-section $x/D = 0.25$, the SSM yields a much higher fluctuating velocity than the IMM does. At $x/D = 0.75$, the influence of the wall treatment is significant. The effects of the wall boundary treatment and the SGS models are of the same order. The significance of these findings has to be further studied in terms of spatial resolution and the turbulent flow field under consideration. It may be expected, as argued above, that the importance of the wall treatment will diminish more quickly than the effect of the SGS model as the grid is refined, very close to the wall. For engineering applications, with modest spatial resolution, the effects of the wall treatment are not negligible.

One of the most important features of swirling flows is the vortex breakdown phenomenon [29]. Due to the centrifugal forces, swirling flows tend to push out fluid towards the edge of the swirling jet, and thereby sucking fluid upstream close to the center-line. The time-average of the flow field yields a recirculation zone near the center-line of the swirling jet inlet. The formation and the shape of the recirculation zones depend on parameters such as the swirl number, the momentum ratio of the axial flow in the central circular inlet and the axial component of the toroidal-annular flow [27,30], and the distance to a side wall. It is interesting to assess the effects of the wall treatment and SGS model on the recirculation zone. Figure 10 shows the recirculation zones, axial velocity component negative, shown in the figure as the darkest regions, calculated using different wall treatment methods with the two SGS models, IMM and SSM respectively. As seen, all the calculations predict a similar near-wall recirculation zone. However, the near-axis recirculation region, the vortex breakdown recirculation, is fairly differently predicted in the different calculations. Using step-wall treatment and IMM, the recirculation zone is at the axis (the first figure from the top). With IMM and high-order wall treatment, on the other hand, a toroidal-(annular) shaped recirculation zone off the cylinder axis is found (the second figure from the top). Using the SSM model with or without high-order wall treatment yields a smaller recirculation zone as compared with the IMM case and the recirculation zones are found at the cylinder axis. The effect of the wall treatment is significant, since the size of the recirculation zone at the axis is considerably larger when the higher-order wall treatment is used.

Experimental results of reacting flows in a similar configuration confirmed the occurence of both the central recirculation zone and the toroidal-shaped recirculation zone off the

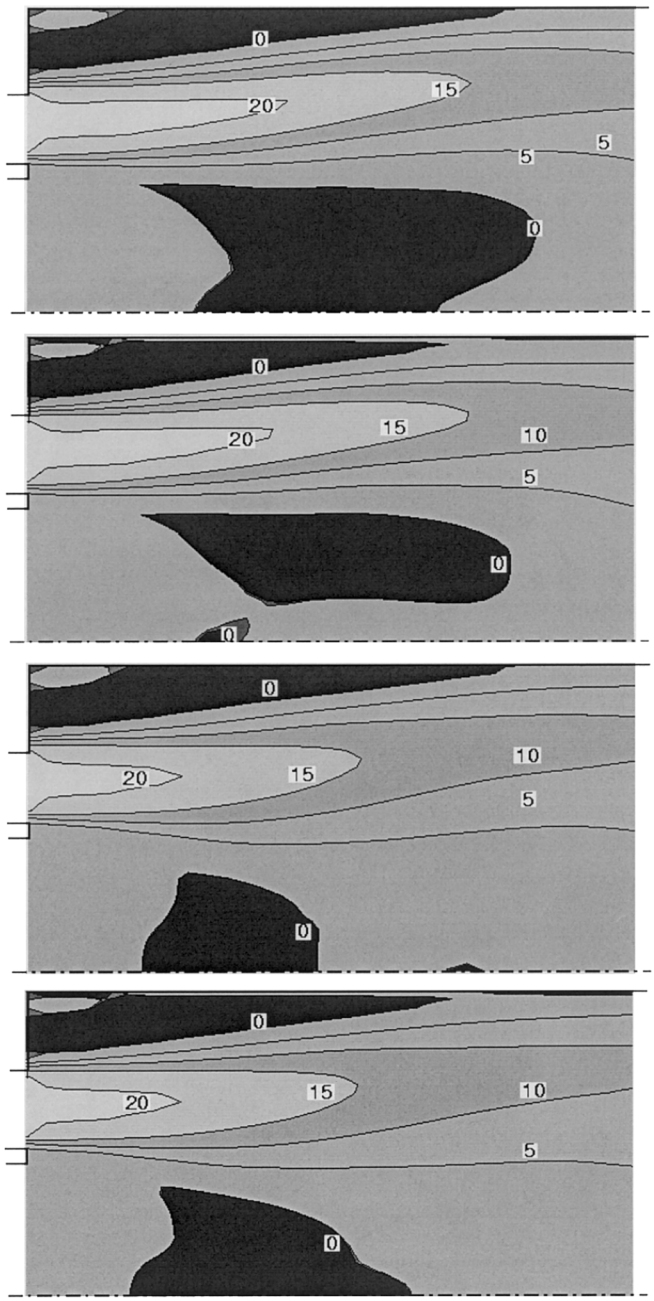

Figure 10. Time-averaged mean axial velocity field computed using different wall treatment methods and SSM models (test case 3). From top to bottom, step wall with IMM, high-order wall with IMM, step wall with SSM and high-order wall with SSM.

cylinder axis [27]. For low swirl number no such recirculation region exists. For increasing swirl numbers a separation bubble is generated. Recent experiments of isothermal flow of co-annular swirling flow into a combustor model has been reported by Xia *et al.* [31]. These experiments also demonstrate clearly the presence of a toroidal recirculation zone. In that particular geometry one may also observe a 'central reverse zone' that is connected to the toroidal zone. The paper of Xia *et al.* [31] also gives numerical results using both two-equation models as well as a Reynolds stress transport model. The problem is rather sensitive to boundary data and even the 'best' (the Reynolds stress transport) model is not very accurate.

Further experiments by Billant *et al.* [32] for low Reynolds number flows, $600 < Re < 1200$ have shown that in addition to a bubble, one may also observe a non-stationary cone. The change between these two states takes place with hysteresis. As the swirl number is further increased, the low pressure obtained at the cone-envelop stretches the central bubble out, which ultimately results in a toroidal recirculation region. Since the computed flow conditions are not identical to the experiments discussed above, it is not possible to conclude which of the above calculations are more correct. Such an assessment is desirable, for which a well-documented experimental set-up and detailed measurement are required.

5. SUMMARY AND CONCLUSIONS

A higher-order wall treatment for a Cartesian grid based numerical method has been introduced for calculation of incompressible turbulent flows. The method utilizes uniformly distributed rectangular Cartesian grids. Therefore, it is easy to construct high-order accurate spatial discretization. Together with isotropic and non-isotropic local grid refinements, and the higher numerical efficiency of Cartesian grids, the approach is appropriate for LES of turbulent flows. The accuracy and the significance of the higher-order wall treatment as compared to SGS models for LES have been investigated.

By using simple test cases, it is easy to show that the higher-order wall treatment yields indeed the expected accuracy. The numerical method has further been applied for LES of a developing isothermal turbulent swirling flow in a cylindrical combustion chamber geometry. The high-order wall treatment yields significantly different results from a low-order piecewise constant step-wall treatment. Two different types of SGS stress models, a SSM and an IMM, have been used. It is shown that the difference of the results using the SSM and IMM may not be much larger than the difference caused by the wall treatment methods. This conclusion is significant if the effort spent on the SGS model development is compared to the effort spent on improving the treatment of boundary conditions.

ACKNOWLEDGMENTS

This work was sponsored by the Swedish Board for Technical and Industrial Development (NUTEK), the Brite-Euram project LES4LPP (EC contract BRPR-CT95-0109) and the CECOST research and graduate school program.

APPENDIX A. IMPROVED ACCURACY BY A SINGLE/FEW STEPS DEFECT CORRECTION

The aim of the method is to compute a higher-order solution to the differential problem using one or a sequence of lower-order approximations. This method is of interest when the lower-order solver has more desirable numerical properties, such as better stability and convergence properties, as compared to the higher-order approximation.

Denote the basic problem that has to be solved by

$$L\Phi = f(x, y)$$

with appropriate boundary conditions.The two discrete approximations to L on the grid with the spacing h are L_1^h and L_2^h. L_1^h is of order q_1 and L_2 is of order q_2, where $q_1 < q_2$.

The basic defect correction scheme is as follows:

Step 1: Solve the following problem for $\Phi^{(1)}$

$$L_1^h \Phi^{(1)} = f(x, y)$$

Step 2: Given $\Phi^{(n)}$, solve the equation for $\Phi^{(n+1)}$

$$L_1^h \Phi^{(n+1)} = f(x, y) + L_1^h \Phi^{(n)} - L_2^h \Phi^{(n)}$$

Step 2 is repeated until $\left|\Phi^{(n+1)} - \Phi^{(n)}\right| < \delta$, where δ is a prescribed small number.

It should be noted that if and when the iteration procedure converges, the solution $\Phi^* = \lim_{n \to \infty} \Phi^{(n)}$ satisfies the following equation

$$L_2^h \Phi^* = f(x, y)$$

which is the equation that wanted to be solved.

The minimal number n for which the final solution will be of the order q_2 for given orders of q_1 and q_2 is

$$n \geq \frac{q_2}{q_1}$$

Proof

By induction. Suppose that at step n, the accuracy of the solution is p and $p = nq_1$. That is

$$\Phi^{(n)} = \Phi^* + h^p g$$

Using the definition of the defect correction, Step 2

$$L_1^h\Phi^* + L_1^h h^m g = f(x, y) + L_1^h\Phi^* + L_1^h h^p g - (L_2^h\Phi^* + L_2^h h^p g)$$

where m is the order of the new approximation, to be shown to be equal to $m = (n+1)q_1$.

By gathering the terms, the expression is

$$L_1^h h^m g = f(x, y) - L_2^h\Phi^* + L_1^h h^p g - L_2^h h^p g$$

which leads to the following estimate:

$$O(h^m) = O(h^{q_2}) + O(h^{p+q_1}) + O(h^{p+q_2})$$

where the first term on the right hand side comes from the discretization L_2^h, the middle and last term account for the difference in the order of approximation of the L_1^h and the L_2^h operator. Thus

$$m = \min[q_2, p+q_1, p+q_2]$$

But since $q_2 > q_1$ and by assertion $p = nq_1$, it is

$$m = \min[(n+1)q_1, q_2]$$

This relation implies that it is meaningful to repeat Step 2, as long as $nq_1 < q_2$.

Assume that the base solution is of second-order, $q_1 = 2$, and that the accuracy of the solution after the first step is also two. The impact of the results is that by solving a new problem, with a slightly different right hand side, once or twice, fourth-order and sixth-order accuracy may be obtained respectively. It should be noted that these solutions are faster to get, in most cases, than the initial one, since the approximation of the initial solution in the later steps of the defect correction algorithm, Step 2, is already of good accuracy. □

REFERENCES

1. Smagorinsky J. General circulation experiments with the primitive equations. *Monthly Weather Review* 1963; **91**: 99–152.
2. Bardina J, Ferziger JH, Reynolds WC. Improved subgrid scale models for large eddy simulation. AIAA Paper 80-1357, 1980.
3. Liu S, Meneveau C, Katz J. On the properties of similarity subgrid-scale models as deduced from measurements in a turbulent jet. *Journal of Fluid Mechanics* 1994; **275**: 83–119.
4. Germano M, Piomelli U, Moin P, Cabot W. A dynamic subgrid-scale eddy viscosity model. *Physics and Fluids A* 1991; **3**: 1760–1765.
5. Germano M, Piomelli U, Moin P, Cabot W. Erratum: a dynamic subgrid-scale eddy viscosity model. *Physics and Fluids A* 1991; **3**: 3128.
6. Clark RA, Ferziger JH, Reynolds WC. Evaluation of subgrid-scale models using an accurately simulated turbulent flow. *Journal of Fluid Mechanics* 1979; **91**: 1–16.
7. Fureby C, Tabor G, Weller HG, Gosman AD. A comparative study of subgrid scale models in homogeneous isotropic turbulence. *Physics and Fluids* 1997; **9**(5): 1416–1429.

8. Ghosal S. An analysis of numerical errors in large eddy simulation of turbulence. CTR Manuscript 159, Center for Turbulence Research, Stanford, 1996.
9. Quirk JJ. An alternative to unstructured grids for computing gas dynamic flows around arbitrarily complex two-dimensional bodies. *Computers and Fluids* 1994; **23**(1): 125–142.
10. Pember RB, Bell JB. An adaptive Cartesian grid method for unsteady compressible flow in irregular regions. *Journal of Computational Physics* 1995; **120**: 278–304.
11. Forrer H, Jeltsch R. A higher order boundary treatment for Cartesian grid methods. *Journal of Computational Physics* 1998; **140**: 259–277.
12. Gullbrand J, Bai XS, Fuchs L. Large eddy simulation of turbulent reacting flows using Cartesian grid and boundary corrections. AIAA Paper 98-3317, 1998.
13. Ferziger JH, Peric M. *Computational Methods for Fluid Dynamics*. Springer: Berlin, 1996.
14. Morton KW, Mayers DF. *Numerical Solution of Partial Differential Equations*, *An Introduction*. Cambridge University Press: Cambridge, 1994.
15. Aftosmis MJ, Melton JE, Berger MJ. Adaptation and surface modeling for Cartesian mesh methods. AIAA Paper 95-1725-CP, 1995; 881–891.
16. Johansen H, Colella P. A Cartesian grid embedded boundary method for Poisson's equation on irregular domains. *Journal of Computational Physics* 1998; **147**: 60–85.
17. Coirier WJ, Powell KG. An accuracy assessment for Cartesian mesh approaches for the Euler equations. AIAA Paper 93-335-CP, 1993; 423–437.
18. Fuchs L. A local mesh-refinement technique for incompressible flows. *Computers and Fluids* 1986; **14**: 69–81.
19. Li Y, Fuchs L. An anisotropic local grid refinement method for fluid flow simulation. *Numerical Heat Transfer* 1996; **30**: 195–215.
20. Pierce CD, Moin P. Large eddy simulation of a confined coaxial jet with swirl and heat-release. AIAA Paper 98-2892, 1998.
21. Boris JP, Grinstein FF, Oran ES, Kolbe RJ. New insights into large eddy simulation. *Fluid Dynamics Research* 1992; **10**: 199–227.
22. Piomelli U, Chasnov JR. Large eddy simulations: theory and applications. In *Turbulence and Transition Modeling*, Hallback M, Henningson DS, Johansson AV, Alfredsson PH (eds). Kluwer Academic Publishers: Dordrecht, 1996; 269–336.
23. Kawamura T, Kuwahara K. Computation of high Reynolds number flow around a circular cylinder with surface roughness. AIAA Paper 84-0340, 1984.
24. Brandt A. Multi-level adaptive solutions to boundary value problems. *Mathematics in Computers* 1977; **31**: 333–390.
25. Fuchs L, Zhao HS. Solution of three-dimensional viscous incompressible flows by a multi-grid method. *International Journal for Numerical Methods in Fluids* 1984; **4**: 539–555.
26. Bai XS, Fuchs L. Fast multigrid method for 3-D turbulent incompressible flows. *International Journal for Numerical Methods in Heat and Fluid Flow* 1992; **2**: 127–137.
27. Owen FK, Spadaccini LJ, Bowman CT. Pollutant formation and energy release in confined turbulent diffusion flames. In *16th Symposium (Int.) on Combustion*. The Combustion Institute: Pittsburgh, 1976; 105–117.
28. Liu C, Liu Z. High order finite difference and multi-grid methods for spatially-evolving instability. *Journal of Computational Physics* 1993; **106**: 265–274.
29. Shtern V, Hussain F. Hysteresis in swirling jets. *Journal of Fluid Mechanics* 1996; **309**: 1–44.
30. Cheng TS, Chao YC, Wu DC, Yuan T, Lu CC, Cheng CK, Chang JM. Effect of fuel–air mixing on flame structures and NO_x emissions in swirling methane jet flames. In *27th Symposium (Int.) Combustion*. The Combustion Institute: Pittsburgh, 1998; 1229–1237.
31. Xia JL, Yadigaroglu GY, Liu YS, Schmidli J. Numerical and experimental study of swirling flow in a model combustor. *International Journal of Heat and Mass Transfer* 1998; **41**: 1485–1497.
32. Billant P, Chomza J-M, Huerre P. Experimental study of vortex breakdown in swirling jets. *Journal of Fluid Mechanics* 1998; **376**: 183–219.

